Metastable Boundary Conditions of Water-in-Oil Emulsions in the Hydrate Formation Region

Jun Chen, Chang-Yu Sun, Bei Liu, Bao-Zi Peng, Xiu-Lin Wang and Guang-Jin Chen
State Key Laboratory of Heavy Oil Processing, China University of Petroleum, Beijing 102249, P. R. China

Julian Y. Zuo and Heng-Joo Ng
DBR Technology Center, Schlumberger, 9450-17 Ave, Edmonton, AB, Canada T6N 1M9

DOI 10.1002/aic.12726
Published online July 25, 2011 in Wiley Online Library (wileyonlinelibrary.com).

A stepwise pressurization method was proposed for determining the metastable boundary conditions of water-in-oil emulsions in the hydrate formation region. The metastable boundary pressures of four water-in-n-octane emulsions in the presence of methane gas were determined at four specified temperatures. The experimental results show that the metastable boundary pressures increase with decreasing water droplet sizes. A thermodynamic model was developed for calculating the metastable boundary conditions of a water-in-oil emulsion in which assuming that the collapse of a metastable emulsion requires the formation of a stable hydrate film with a critical thickness on the surfaces of water droplets. The model was used to correlate the experimental data and determine the critical thickness of the hydrate film. It was demonstrated that the calculated results were in good agreement with the experimental data. The determined critical thickness is at nanoscale, ranging from 14 to 40 nm, which decreases with decreasing water droplet sizes. © 2011 *American Institute of Chemical Engineers AIChE J,* 58: 2216–2225, 2012
Keywords: emulsion, metastable boundary, hydrate, methane, film

Introduction

Gas hydrates are ice-like solids formed by the insertion of guest molecules into cage-like crystalline lattices of host water molecules at elevated pressures and low-temperatures. In the past decades, most fundamental studies on gas hydrates have focused on hydrate formation/dissociation from bulk water. However, in oil and gas production and transportation, hydrate formation in dispersed aqueous systems such as water-in-oil emulsions often occurs. For example, when surface-active antiagglomerants are added to prevent pipelines from being plugged by hydrates, hydrates usually form from water-in-oil emulsions.[1] Even though there are no antiagglomerants added, the naturally occurring surface-active compounds such as asphaltenes in crude oil may also give rise to forming water-in-oil emulsions in some multiphase flow systems.[2] Furthermore, most drilling fluids in deepwater offshore drilling facilities, where hydrate plugging hazards may occur because of low seabed temperatures, are in forms of water-in-oil emulsions.[3] Hence, understanding the characteristic of hydrate formation in water-in-oil emulsions has drawn much attention in recent years.[4–14]

With in-depth studies on hydrate formation/dissociation in water-in-oil emulsions, the relevant experimental techniques such as the differential scanning calorimetry (DSC),[3,5–8] X-ray diffraction,[9,10] nuclear magnetic resonance (NMR),[11] particle video microscope (PVM), focused beam reflectance measurement (FBRM),[12] and dielectric spectroscopy[13,14]have been used to characterize hydrate formation in water-in-oil emulsions. Dalmazzone et al.[5] measured the dissociation of methane hydrate in water-in-oil emulsion systems using the DSC technique and pressure vs. temperature measurements in a constant volume cell (pressure–volume–temperature, PVT). Both DSC and PVT results showed that there are no measurable differences between the bulk solutions and emulsions from the thermodynamic point of view. Therefore, the attention of hydrate researches in water-in-oil emulsions has been paid to other directions because the thermodynamic difference between bulk solutions and emulsions has been thought to be negligible. Aichele et al.[11] analyzed methane hydrate formation in water-in-oil emulsions through the NMR technique. They showed some quantitative information about the relationship between water droplet-size distributions and methane hydrate formation. In addition, Boxall et al.[12] studied the gas hydrate formation and dissociation in water-in-oil emulsions by using the PVM and FBRM. They concluded that water droplet sizes had a major effect on whether or not agglomeration would occur. The presence of surface water on the particles can facilitate the agglomeration of hydrates during dissociation. From the studies of Aichele et al.[11] and Boxall et al.,[12] it can then be found that water droplet sizes affect both hydrate formation and agglomeration.

Hydrate particles at nanoscale formed from the micro-droplets of water in an emulsion usually tend to

Correspondence concerning this article should be addressed to G.-J. Chen at gjchen@cup.edu.cn; C.-Y. Sun at cysun@cup.edu.cn

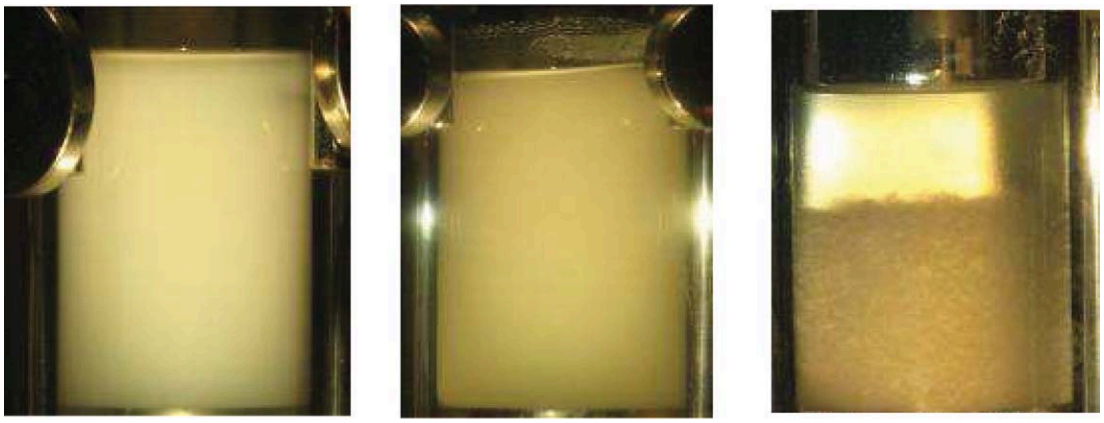

Figure 1. The process of hydrate formation from a water-in-*n*-octane emulsion: (a) stable emulsion; (b) initiation of hydrate formation; (c) mass hydrate particles of macroscopic sizes.

[Color figure can be viewed in the online issue, which is available at wileyonlinelibrary.com.]

agglomerate into larger ones to lower their surface free energies because of the larger interfacial tension between hydrate and oil. This phenomenon has been observed frequently in our experimental work, as shown in Figure 1. The agglomerated hydrate particles might be of macroscopic size and then the interfacial tension has little effect on the equilibrium dissociation conditions. That might explain why the equilibrium hydrate formation/dissociation conditions in a water-in-oil emulsion system is the same as that in the bulk aqueous phase.[5] However, the initial nucleation of hydrate from a small water droplet, e.g., a water droplet with a diameter of less than 500 nm, might be more difficult than that from a large water droplet because of the higher-surface-free energy of hydrate film formed on the surface of the water droplet. This means that a water droplet in a water-in-oil emulsion should be of a wider stable liquid phase region than bulk water within which stable nucleation of hydrate is impossible, although it is the rigorously metastable one. From the technical point of view, one can then inhibit hydrate formation by forming w/o emulsion with water droplet size small enough. The objective of this work is to investigate the metastable boundary conditions of water-in-oil emulsions in the hydrate formation region, i.e., the initial hydrate formation conditions in water-in-oil emulsion systems.

Experimental Section

Experimental apparatus and materials

The schematic diagram of the experimental apparatus used in this work for measuring the initial hydrate formation conditions in water-in-oil emulsion was shown in Figure 2. It mainly contains a sapphire cell and an air bath. The detailed descriptions of this apparatus can be referred to our previous works.[15–17]

Analytical grade (99.99%) methane supplied by the Beifen Gas Industry Corporation was used in this work. Sorbitan monolaurate (Span 20), nonylphenol ethoxylates, and *n*-octane were purchased from the Beijing Chemical Reagents Company. The water was distilled twice and its conductivity is less than 10^{-4} S m^{-1}.

Preparation of emulsions

The quantities of water, *n*-octane, nonylphenol ethoxylates, and Span 20 used to prepare the emulsion were respectively weighed with a balance possessing a precision of 0.1 mg. The emulsion was prepared through stirring the mixture of water, *n*-octane, nonylphenol ethoxylates, and Span 20 with a specified composition by using the ULTRA TURRAX T-18 disperser manufactured by the IKA corporation in German. The size (diameter) distribution and average size of water droplets in the emulsion were measured by virtue of the Zetasizer Nano-ZS laser nanoparticle-size analyzer manufactured by the Britain Malvern Instruments. The diameter range measured by the analyzer can be from 0.6 to 6000 nm. Four different types of water-in-*n*-octane emulsions denoted by $1^{\#}$, $2^{\#}$, $3^{\#}$, and $4^{\#}$ were prepared. The dosages of the surfactants added and the details of the emulsion preparations were listed in Table 1. The water droplet diameter distributions of four emulsions were measured at 293.2 K before hydrate formation, and the results were shown in Figure 3. Except for the main peak, we found a small peak in Figures 3a, b. It might be caused by the impurity in

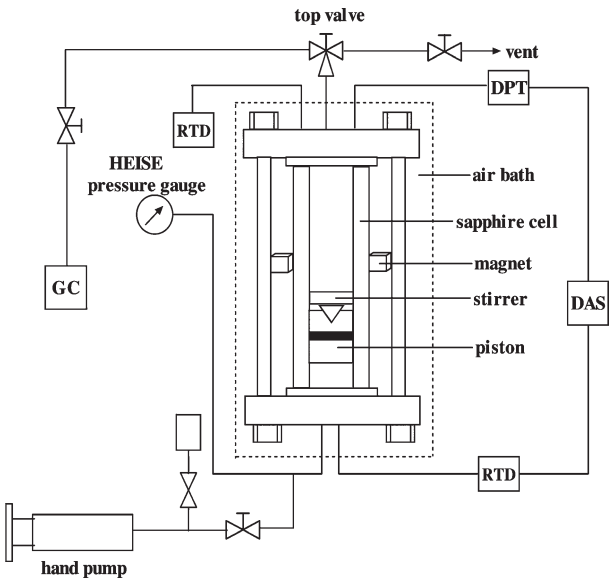

Figure 2. Schematics of the experimental apparatus: RTD, resistance thermocouple detector; DPT, differential pressure transducer; GC, gas cylinder; DAS, data acquisition system.

Table 1. The Information of Emulsion Preparations

Emulsion No.	Water Cut (v %)	The Dosage of Surfactant Mixture (A + B)* in Water (wt %)	Mixing Speed (rpm)	Mixing Time (min)
1#	10	3.9	6000	6
2#	20	3.0	6000	6
3#	30	3.0	7200	6
4#	30	3.0	6000	6

*The mass ratio of A (Span 20) to B (nonylphenol ethoxylates) in the surfactant mixture is 2:1.

measuring systems. For 4#emulsion, there exist two peaks, indicating that part of small water droplets agglomerate into larger ones. The average diameters of water droplet for the two peaks are 691.2 nm (peak A) and 4342 nm (peak B), respectively. The obtained average diameter of water droplet of emulsion and standard deviation were listed in Table 2 correspondingly.

Activation and recovery of emulsions

The sapphire cell was loaded with about 20 mL of the prepared emulsion and installed onto the apparatus. Then methane gas was introduced into the cell until the desired pressure was achieved. The system temperature and pressure were adjusted to form and dissociate hydrate repeatedly to eliminate the induction time of hydrate nucleation. After the last round of hydrate formation and dissociation, the system was depressurized to atmospheric pressure, heated to 298 K, and agitated with the stirrer for more than 1 h to guarantee the absence of hydrate particles and recover the stable homogeneous emulsion.

Determination of metastable boundary conditions of emulsions

After the activation and the recovery of the emulsion, the system temperature was adjusted to a given value, and methane gas was charged into the sapphire cell again until the pressure was close to the equilibrium pressure of hydrate formation/dissociation in bulk water at present temperature. During the whole measurement, the emulsion was agitated with the magnetic stirrer continuously. Once the temperature was stabilized, the pressure in the cell was then adjusted to this equilibrium pressure with the piston in the cell and stabilized at that value for 24 h. If hydrate formation was not observed during this time period, the system pressure was increased by 0.1 MPa or so, and the cell was kept stirring for another 24 h. If hydrate formation was not observed still, the system was pressurized step by step and stabilized for 24 h in each step until a sudden drop of pressure was observed, as shown in Figure 4. The pressure step was set to about 0.1 MPa during the pressurization. The sudden drop of pressure manifests the formation of hydrate and the destruction of emulsion. In this work, the average value of the pressure at the final step and that at the previous one was defined as the metastable boundary pressure of the emulsion at a given temperature, which is denoted as P_m in Figure 4. Thus, the uncertainty of P_m measurement is 0.05 MPa. After the P_m value at one specified temperature was determined, the system was depressurized to atmospheric pressure and heated to above 298

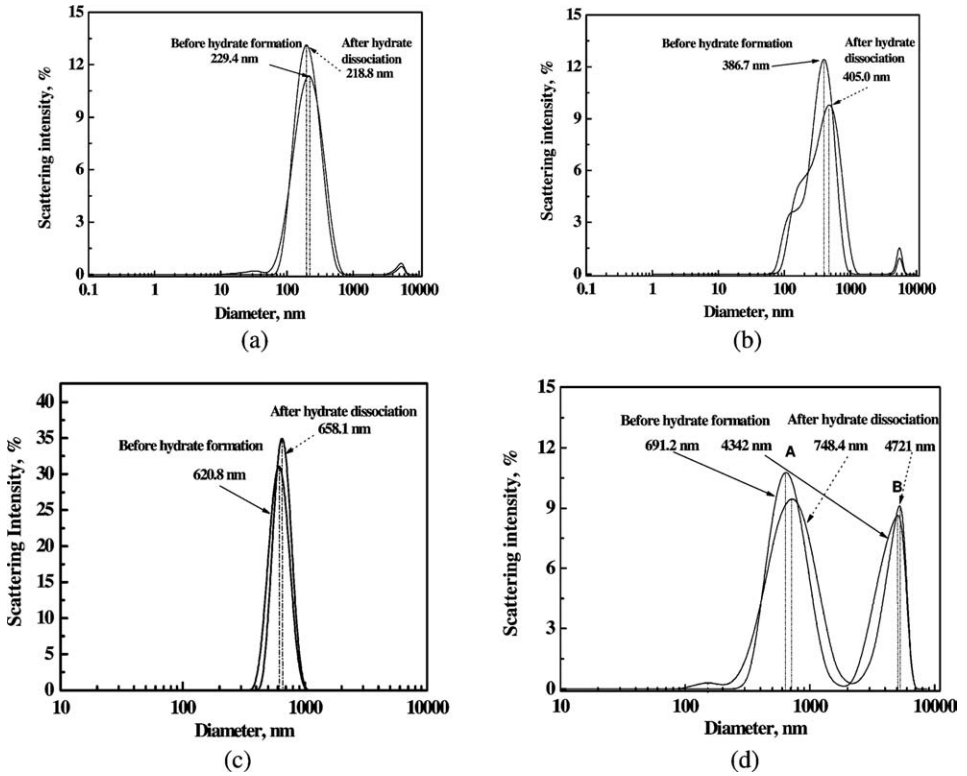

Figure 3. Comparison of the water droplet diameter distributions before and after repeated hydrate formation/dissociation: (a) 1# emulsion; (b) 2# emulsion; (c) 3# emulsion; (d) 4# emulsion.

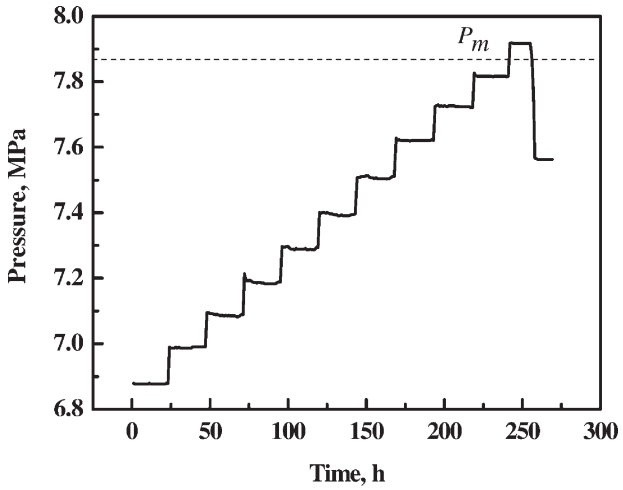

Figure 4. The path of pressurization during searching the metastable boundary pressure of the 1# water-in-*n*-octane emulsion system at 282.15 K.

K to dissociate the hydrate thoroughly and recover the stable emulsion for the next measurement.

Measurement of droplet-size distribution after hydrate formation /dissociation

After the metastable boundary pressures of a specified water-in-oil emulsion at a series of specified temperatures were determined, the recovered emulsion in the cell was sampled and the diameter distribution of the water droplets in the emulsion was analyzed with the Nano-ZS laser nanoparticle-size analyzer to determine the effect of repeated formation/dissociation of hydrate on structures of the emulsion.

Modeling of Metastable Boundary Conditions

There exist many models for predicting the hydrate formation conditions in bulk phase[18–24] or in porous media.[25–28] However, there is no thermodynamic model reported for calculating the metastable boundary conditions of a water-in-oil emulsion. Taylor et al.[29] proposed a mechanism for the conversion of a water droplet into hydrate. They suggested that the first stage of hydrate nucleation is a hydrate film propagating around the water droplet. Our modeling work is also based on this mechanism. It is assumed that collapse of a metastable emulsion requires formation of stable hydrate films with a critical thickness r_c on the surfaces of water droplets, and that the chemical potential of hydrate lattice must be low enough to equilibrate with that of the residual water droplet enclosed by the hydrate film, as shown in Figure 5. The surface-free energy should be taken into account when formulating the Gibbs free energies of both water droplet and hydrate film because the water droplet size and the thickness of the hydrate film are close to or at nanoscale. There exists an interface, the water/oil interface, before the formation of hydrate film while there exist two interfaces, i.e., the oil/hydrate interface and the hydrate/water interface, after the formation of hydrate film. The Gibbs free energy of water droplet before the hydrate formation can be formulated as

$$G_{\text{droplet}} = n_{w0}\mu_w^{\text{bulk}} + 4\pi r_0^2\sigma^{W-O} \tag{1}$$

where μ_w^{bulk} is the chemical potential of bulk water, n_{w0} is the molar number of water in the initial water droplet, r_0 is the radius of initial water droplet, and $\sigma^{W\text{-}O}$ is the water/oil interfacial tension.

The Gibbs free energy of water droplet plus hydrate film, G_M, after the hydrate formation can be formulated as

$$G_M = n_w\mu_w^{\text{bulk}} + \Delta n_w\mu_B^{\text{bulk}} + 4\pi r^2\sigma^{H-W} + 4\pi(r+r_c)^2\sigma^{H-O} \tag{2}$$

where μ_B^{bulk} is the chemical potential of bulk basic hydrate, n_w is the molar number of water in the residual water droplet, and Δn_w is the molar number of water molecules in hydrate film

$$n_w = n_{w0} - \Delta n_w \tag{3}$$

σ^{H-W} and σ^{H-O} denote the interfacial tension of hydrate/water and hydrate/oil, respectively. According to the literature,[30] σ^{H-W} is set to 17 mN m^{-1} in the calculation. σ^{H-O} is taken as the sum of σ^{H-W} and σ^{O-W}. In this work, the interfacial tensions of *n*-octane/water, σ^{O-W}, were measured in the presence of different dosages of surfactants as shown in Table 1 using the "pendant-drop" method.[31] Under these experimental conditions, they are all 4.0 mN m^{-1} because the dosages of surfactants are higher than the critical micelle concentration. r is the radius of the residual water droplet. r_c is the critical thickness of hydrate film, which is taken as an adjustable parameter determined by fitting the experimental data. The relation between r and the initial radius of the water droplet r_0 is given by

$$(r+r_c)^3 - r^3 = 1.25(r_0^3 - r^3) \tag{4}$$

where coefficient 1.25 is the ratio of the molar volume of the empty hydrate lattice to that of water.

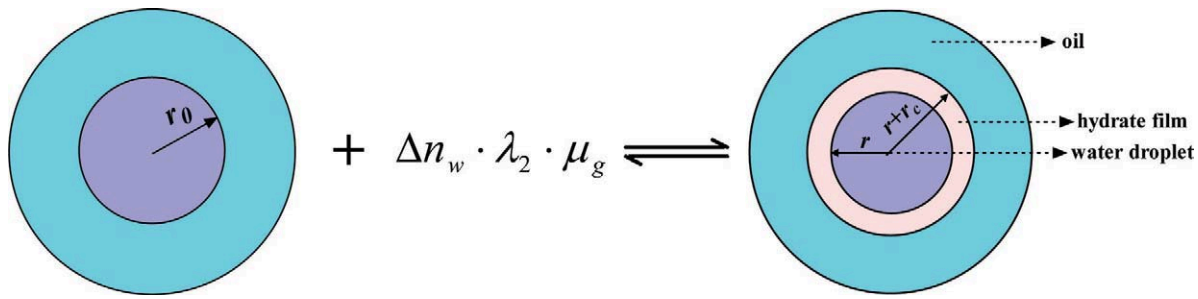

Figure 5. The schematics of the equilibrium process of the formation basic hydrate film from a water droplet and gas component in a w/o emulsion system.

[Color figure can be viewed in the online issue, which is available at wileyonlinelibrary.com.]

The definition of basic hydrate can be referred to Chen and Guo.[22] μ_B^{bulk} can be expressed as,[23]

$$\mu_B^{bulk} = \mu_B^0 + \lambda_1 RT(1-\theta) \tag{5}$$

where θ is the fraction of the small cavities occupied by gas molecules, which can be calculated by the Langmuir isothermal adsorption theory. μ_B^0 is the chemical potential of unfilled basic hydrate lattice (θ = 0). λ_1 denotes the number of small cavity per water molecules in the hydrate lattice.

If the hydrate formation illustrated in Figure 5 is a reversible process as we concerned in this work, the variation of Gibbs free energy of this process should be equal to zero. That is, Gibbs free energy of the initial water droplet plus that of hydrate forming gas should be equal to the Gibbs free energy G_M, i.e.,

$$n_{w0}\mu_w^{bulk} + 4\pi r_0^2\sigma^{W-O} + \Delta n_w\lambda_2\mu_g = n_w\mu_w^{bulk} + \Delta n_w\mu_B^{bulk} + 4\pi r^2\sigma^{H-W} + 4\pi(r+r_c)^2\sigma^{H-O} \tag{6}$$

where μ_g is the chemical potential of gas and λ_2 is the molar number of large cavities per mole basic hydrate.

It can be derived from the above equation that

$$\mu_w^{bulk} + \lambda_2\mu_g = \mu_B^{bulk} + 4\pi[r^2\sigma^{H-W} + (r+r_c)^2\sigma^{H-O} - r_0^2\sigma^{W-O}]/\Delta n_w \tag{7}$$

$$\Delta n_w = \frac{4}{3}\pi[(r+r_c)^3 - r^3]/V_H^0 \tag{8}$$

where V_H^0 is the molar volume of the empty hydrate lattice. Substituting Eq. 8 into Eq. 7, we obtain,

$$\mu_w^{bulk} + \lambda_2\mu_g = \mu_B^{bulk} + 3V_H^0[r^2\sigma^{H-W} + (r+r_c)^2\sigma^{H-O} - r_0^2\sigma^{W-O}]/[(r+r_c)^3 - r^3] \tag{9}$$

To simplify Eq. 9, an effective activity of water (a_w) related to the capillary effect on the hydrate formation condition is defined as

$$RT\ln a_w = -3V_H^0[r^2\sigma^{H-W} + (r+r_c)^2\sigma^{H-O} - r_0^2\sigma^{W-O}]/[(r+r_c^3) - r^3] \tag{10}$$

Equation 9 then becomes

$$\mu_w^{bulk} + RT\ln a_w + \lambda_2\mu_g = \mu_B^{bulk} \tag{11}$$

The chemical potential of gas component (μ_g) can be expressed as a function of gas fugacity (f),

$$\mu_g = \mu_g^0(T) + RT\ln f \tag{12}$$

Substituting Eqs. 5 and 12 into Eq. 11, we have,

$$\mu_w^{bulk} + RT\ln a_w + \lambda_2(\mu_g^0(T) + RT\ln f) = \mu_B^0 + \lambda_1 RT\ln(1-\theta) \tag{13}$$

To simplify Eq. 13, an auxiliary function (f^0) was defined as[23]

$$f^0 = \exp\left[\frac{\mu_B^0 - \mu_w^{bulk} - \lambda_2\mu_g^0(T)}{\lambda_2 RT}\right] \tag{14}$$

Equation 13 is then rewritten as

$$f = f^0(1-\theta)^\alpha a_w^{-1/\lambda_2} \tag{15}$$

where λ_1 and λ_2 denote the number of small cavity and large cavity per water molecules in the hydrate lattice. $\alpha = \lambda_1/\lambda_2$, $\lambda_2 = 3/23$, and $\alpha = 1/3$ for structure I hydrate, e.g., methane hydrate concerned in this work. The method for calculating f_0 can be referred to Chen and Guo.[23]

Results and Discussion

The metastable boundary pressures of the four emulsions described in Table 1 in the presence of methane gas were determined, respectively, at four different temperatures according to the procedures described previously. The experimental results were tabulated in Table 3 and shown in Figure 6. For comparison, the equilibrium formation pressures of methane hydrate from bulk water[32] were also listed in Table 3 correspondingly. A typical pressurization path during single measurement was shown in Figure 4. Other pressurization paths were given in Appendix. As shown in Figure 4 and Appendix, search of metastable boundary pressure of an emulsion is time consuming. A single search usually takes several days. As expected, P_m increases with increasing temperature monotonously for a specified emulsion. The scattering of P_m values is very low, which manifests that the value of P_m is determined thermodynamically instead of kinetically. More importantly, P_m increases with decreasing water droplet sizes of the emulsion, which demonstrates that hydrate formation from a microdroplet of water in a water-in-oil emulsion is more difficult than from bulk water. The smaller the water droplet size is, the more difficult to form hydrate and the wider the metastable region of the emulsion will be. Obviously, the effect of interfacial tension on the initial hydrate formation conditions of a water-in-oil emulsion should be taken into account when the metastable boundary conditions of the emulsion are modeled. This was also affirmed from the metastable boundary pressure of 4#emulsion. For 4#emulsion, some water droplets with small diameter may agglomerate into large ones due to the high-water-cut of the emulsion. A multimodal-size distribution appears for the size distribution of water droplet diameter, which are 691.2 nm (peak A) and 4342 nm (peak B) before hydrate formation, respectively, as shown in Figure 3d. If we only take water droplet diameter of peak A into consideration, the metastable boundary pressure value of 3#emulsion should be similar to that of 4#emulsion in view that the close initial water droplet diameters of 620.8 nm (3#) and 691.2 nm (peak A for 4#). However, as shown in Table 3, the

Table 2. The Average Diameters of Water Droplet of Emulsions and Standard Deviations Before Hydrate Formation and After Hydrate Formation/Dissociation

	Water Droplet Diameter (nm)		Standard Deviation (nm)	
Emulsion No.	Before Hydrate Formation	After Hydrate Dissociation	Before Hydrate Formation	After Hydrate Dissociation
1#	229.4	218.8	105.5	88.8
2#	386.7	405.0	140.8	210.9
3#	620.8	658.1	96.9	87.7
4# (Peak A)	691.2	748.4	217.7	297.0
4# (Peak B)	4342.0	4721.0	939.3	778.8

Table 3. Metastable Boundary Pressures of Four Emulsions in the Presence of Methane Gas at Four Different Temperatures of 276.15, 278.15, 280.15, and 282.15 K

Number of Emulsion	Temperature (K)	P_m (MPa)
1#	276.15	4.115
	278.15	5.061
	280.15	6.146
	282.15	7.866
2#	276.15	3.915
	278.15	4.718
	280.15	5.955
	282.15	7.204
3#	276.15	3.764
	278.15	4.614
	280.15	5.867
	282.15	7.091
4#	276.15	3.663
	278.15	4.513
	280.15	5.698
	282.15	6.972
Bulk water[32]	276.22	3.55
	278.24	4.33
	280.24	5.31
	282.23	6.53

actual metastable boundary pressure of 3#emulsion is higher than that of 4#emulsion, indicating that the P_m is dependent on the large water droplet of 4#emulsion (peak B for 4#). This can be attributed to the reason that large water droplets have low-surface-free energy and are more easily to form hydrate.

It is interesting to see from Figure 4 and Appendix that the system pressure decreases steeply when hydrate formation occurs, which indicates the collapse of the metastable emulsion because of stable hydrate formation. It also shows that the hydrate growth rate is very fast after the metastable state of the emulsion is destroyed. The formed nanoscale hydrate particles tend to agglomerate with each other rapidly and then become macroscale ones. As shown in Figure 1c, one can clearly see that the opaque emulsion becomes the transparent oil and the hydrate deposition. If the quantity of water is sufficient, the system pressure may decrease to the equilibrium formation/dissociation pressure of methane hydrate. For a comparison of the difference between P_m and the equilibrium hydrate formation pressure, the equilibrium methane hydrate formation pressures for the water-in-*n*-octane emulsion 1# were measured at 276.15 and 282.15 K, respectively. Results are 3.508 MPa and 6.788 MPa, correspondingly. They are only a little higher than the equilibrium formation pressures of methane hydrate from bulk water (3.453 and 6.516 MPa at 276.15 K and 282.15 K, respectively). This kind of difference should be attributed to the presence of surfactants in water, which may lower the activity of water. For the pressurization path of water-in-*n*-octane emulsion 3# at 282.15 K as shown in Figure A3, it can be found that the stable pressure after the formation of hydrate is about 6.741 MPa, which is close to the equilibrium pressures of methane hydrate in surfactant solution. These results demonstrate that P_m is only a kind of metastable boundary pressure of the emulsion instead of the equilibrium hydrate formation pressure. However, it is impossible to form hydrate at pressure lower than P_m unless stable hydrate particles in the emulsion are present. Thus, P_m is one of the thermodynamic conditions for hydrate initiation from a water-in-oil emulsion. To understand this is of significance for predicting hydrate hazards in gas/oil pipelines or drilling fluids.

The water droplet-size distribution of each recovered emulsion after a set of measurements of P_m was analyzed to determine the effect of the repeated formation/dissociation of hydrate on the size distribution of water droplets. The results were shown in Figure 3 and Table 2. As shown in Figure 3 and Table 2, the average water droplet diameters of three emulsions 1#, 2#, and 3# are 229.4, 386.7, and 620.8 nm, respectively before hydrate formation. They become 218.8, 405.0, and 658.1 nm after the repeated formation/dissociation of hydrate occurred in the measurements of P_m. It indicates that the formation and dissociation of hydrate makes the average water droplet size change a little in our work. To evaluate the effect of temperature on water droplet diameter distribution, we have measured the water droplet diameter distribution of one additional emulsion in the temperature range of 276.2 to 298.2 K and found that the average diameter of water droplet increased from 400 to 410 nm. Although these effects increase the uncertainty in measurement of water droplet diameter, their effects on P_m value is negligible with considering the maximum change of P_m is only 0.78 MPa when the water droplet diameter changes from 620.8 to 229.4 nm at a specified temperature, as shown in Tables 2 and 3.

The thermodynamic model established in the previous section was used to correlate the experimental data and then determine the critical thickness of the stable hydrate film. To reduce the influence of the uncertainty in measurement of water droplet size on the calculation result, the water droplet radius r_0 was taken as the average value of that before hydrate formation and after hydrate formation/dissociation in the calculation. The calculation results as well as the average water droplet diameters at different experimental conditions were shown in Figure 6 and Table 4. For water droplet of 4#emulsion, the average diameter indicated by peak B was adopted. One can see that the agreement between the calculated results and the experimental data is satisfying. The average absolute deviation is about 1%. The determined critical thicknesses of the hydrate films for the four different emulsions are 14, 23, 28, and 40 nm, respectively, corresponding to four average water droplet diameters of 224.1, 395.9, 639.5, and 4531.5 nm. It is interesting to see that the critical thickness of the hydrate film decreases with a reduction of the initial water droplet size. This can be attributed to the reason that the specific surface area of the residual water droplets increases

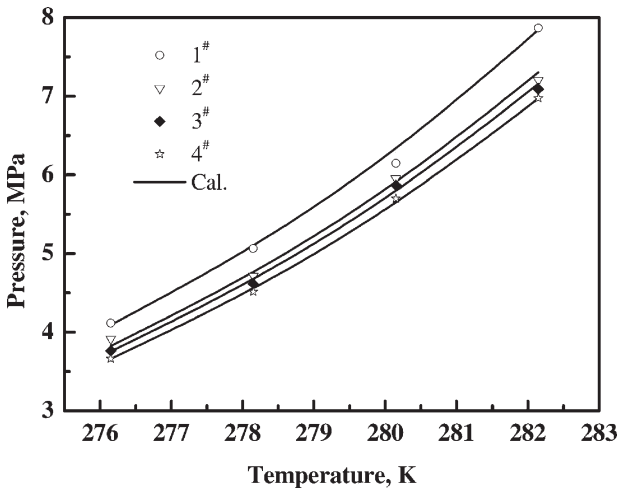

Figure 6. The metastable pressures of four emulsions in the presence of methane gas at different temperatures.

Table 4. Comparison of the Experimental Values with Calculated Results

Emulsion No.	Average Water Droplet Diameter* (nm)	Temperature Range (K)	Pressure Range (MPa)	r_c (nm)	N_p	AADP (%)**
1#	224.1	276.15–282.15	4.115–7.866	14	4	0.78
2#	395.9	276.15–282.15	3.915–7.204	23	4	1.36
3#	639.5	276.15–282.15	3.764–7.091	28	4	0.93
4#	4531.5	276.15–282.15	3.663–6.972	40	4	0.51

*The average value of water droplet diameters of emulsion measured before and after hydrate formation/dissociation.

**AADP is defined as AADP $=\sum_j^{N_p} \left|(P_{cal} - P_{exp})/P_{exp}\right|_j / N_p \times 100\%$

more steeply when the hydrate film formed from the surface of a water droplet with a smaller initial diameter as the specific surface area of the water droplet is proportional to the reverse (reciprocal) of its diameter. For example, the increase of the specific surface area of the residual water droplet is only 7.93% when a hydrate film with a critical thickness of 28 nm forms from the surface of a water droplet with an initial diameter of 620.8 nm. Whereas, when a hydrate film with the same thickness forms from a water droplet with an initial diameter of 229.4 nm, the specific surface area of the residual water droplet will increase by 25.67 %. The steeper increase of the specific surface area will result in a steeper increase of the specific surface free energy or the chemical potential of the residual water droplet. To balance the chemical potential of the residual water droplet and that of the hydrate film, the actual critical thickness of hydrate film must be thinner for a smaller water droplet than for a larger one. Englezos et al.[33] evaluated the critical diameters of hydrate particles formed from bulk water and found they are from 6 to 34 nm. Their results are in the same magnitude as ours. As the metastable boundary pressures increase with the decreasing water droplet sizes of the emulsion, the hydrate film formed from a smaller diameter of water droplet should be under a higher driving force. Therefore, from the relationship between the hydrate film thickness and the driving force by Peng et al.,[34] the hydrate film thickness will also be thinner for a smaller water droplet.

Conclusions

Four water-in-*n*-octane emulsions were prepared by adding suitable dosages of surfactants (Span 20 and nonylphenol ethoxylates with a mass ratio of 2:1) to water + *n*-octane mixtures with different water cuts. The stepwise pressurization method was proposed for determining the metastable boundary conditions of water-in-oil emulsions in the hydrate formation region. The metastable boundary pressures of the four emulsions in the presence of methane gas were then determined at four given temperatures. The experimental data show that the metastable boundary pressure increases with increasing temperature monotonously for a specified emulsion and also increases obviously with a reduction of the water droplet sizes at a given temperature. When the system pressure exceeds the metastable boundary pressure, hydrate formation occurs, and the metastable state of the emulsion collapses. The formed nanosale hydrate particles then tend to agglomerate with each other rapidly and become macroscale ones for decreasing the surface free energy. If the system pressure is lower than P_m, it is impossible to form hydrate unless stable hydrate particles in the emulsion are present.

A thermodynamic model was developed for calculating the metastable boundary conditions of water-in-oil emulsions by assuming that the collapse of metastable emulsions requires the formation of stable hydrate films with a critical thickness on the surfaces of water droplets. In addition, it is assumed that the chemical potential of the hydrate film must be low enough to equilibrate with that of the residual water droplet enclosed by the hydrate film. The model was then used to correlate the experimental data and determine the critical thickness of the hydrate film. The calculated results were in good agreement with the experimental data. The determined critical thickness ranges from 14 to 40 nm which decreases with decreasing water droplet sizes. This finding might be helpful for revealing the mechanism of hydrate nucleation.

The results obtained in this work should be of significance for predicting or preventing hydrate hazards in oil/gas pipelines or petroleum drilling facilities offshore. They reveal that it is more difficult to form hydrate from w/o emulsion than from bulk water, and the difficulty increases with decreasing water droplet size. This finding suggests that one can inhibit hydrate formation by forming w/o emulsion with desirable small water droplet size.

Acknowledgments

The financial support received from the National Natural Science Foundation of China (Nos. 20925623, 21076225), National 973 Project of China (No. 2009CB219504), the Research Funds of China University of Petroleum, Beijing (BJBJRC-2010-01), and Beijing Novel Program (2010B069) are gratefully acknowledged.

Literature Cited

1. Zanota ML, C Dicharry, A Graciaa. Hydrate plug prevention by quaternary ammonium salts. *Energy Fuels.* 2005;19:584–590.
2. Poindexter MK, Zaki NN, Kilpatrick PK, Marsh SC, Emmons DH. Factors contributing to petroleum foaming. 1. Crude oil systems. *Energy Fuels.* 2002;16:700–710.
3. Dalmazzone D, Hamed N, Dalmazzone C. DSC measurements and modeling of the kinetics of methane hydrate formation in water-in-oil emulsion. *Chem Eng Sci.* 2009;64:2020–2026.
4. Fidel-Dufour A, Hong DN, Herri JM. Formation and dissociation of hydrate plugs in a water in oil emulsion. Proceedings of the fourth International Conference on Gas Hydrate. Yokohama, Japan; May 19–23, 2002.
5. Dalmazzone D, Kharrat M, Lachet V, Fouconnier B, Clausse D. DSC and PVT measurement Methane and trichlorofluoromethane hydrate dissociation equilibria. *J Therm Anal Calorim.* 2002;70:493–505.
6. Dalmazzone D, Hamed N, Dalmazzone C, Rousseau L. Application of high pressure DSC to the kinetics of formation of methane hydrate in water-in-oil emulsion. *J Therm Anal Calorim.* 2006;85:361–368.
7. Dalmazzone D, Dalmazzone C, Herzhaff B. Differential scanning calorimetry: a new technique to characterize hydrate formation in drilling muds. *SPE J.* 2002;7:196–202.
8. Fouconnier B, Legrand V, Komunjer L, Clausse D, Bergfoldt L, Sjoblom J. Formation of trichlorofluoromethane hydrate in w/o emulsion studied by differential scanning calorimetry. *Progr Colloid Polym Sci.* 1999;112:105–108.
9. Fouconnier B, Komunjer L, Ollivon M, Lesieur P. Keller G, Clausse D. Study of CCl_3F hydrate formation and dissociation in w/o emulsion by differential scanning calorimetry and X-ray diffraction. *Fluid Phase Equilib.* 2006;250:76–82.
10. Komunjer L, Ollivon M, Fouconnier B, Luong AT, Pezron I, Clausse D. Influence of Sodium chloride on the melting of ice and crystallization and dissociation of CCl_3F hydrate in water in oil emulsion. *J Therm Anal Calorim.* 2009;98:125–131.
11. Aichele CP, Chapman WG, Rhyne LD, Subramani HJ, Montesi A, Creek JL, House W. Nuclear magnetic resonance analysis of methane hydrate formation in water-in-oil emulsions. *Energy Fuels.* 2009;23:835–841.

12. Boxall J, Greaves D, Mulligan J, Koh C, Sloan ED. Gas hydrate formation and dissociation from water-in-oil emulsions studied using PVM and FBRM particle size analysis. Proceedings of the Sixth International Conference on Gas Hydrate. Vancouver, British Columbia, Canada; July 6–10, 2008.
13. Jakobsen T, Sjoblom J, Ruoff P. Kinetics of gas hydrate formation in w/o-emulsions the model system trichlorofluoromethane/water/non-ionic surfactant studied by means of dielectric spectroscopy. *Colloids Surf A*. 1996;112:73–84.
14. Jakobsen T, Folgerø K. Dielectric measurements of gas hydrate formation in water-in-oil emulsions using open-ended coaxial probes. *Meas Sci Technol*. 1997;8:1006–1015.
15. Mei DH, Liao J, Yang JT, Guo TM. Experimental and modeling studies on the hydrate formation of a methane + nitrogen gas mixture in the presence of aqueous electrolyte solutions. *Ind Eng Chem Res*. 1996;35:4342–4347.
16. Mei DH, Liao J, Yang JT, Guo TM. Hydrate formation of a synthetic natural gas mixture in aqueous solutions containing electrolyte, methanol, and (electrolyte + methanol). *J Chem Eng Data*. 1998;43:178–182.
17. Zhang SX, Chen GJ, Ma CF, Yang LY, Guo TM. Hydrate formation of hydrogen + hydrocarbon gas mixture. *J Chem Eng Data* 2000;45:908–911.
18. van der Waals JH, Platteeuw JC. Clathrate solutions. *Adv Chem Phys* 1959;2:1–57.
19. Sloan ED Jr. *Clathrate Hydrates of Natural Gases*, New York: Marcel Dekker, 1998.
20. Yoon JH, Chun MK, Lee H. Generalized model for predicting phase behavior of clathrate hydrate. *AIChE J*. 2002;48:1317–1330.
21. Yoon JH, Yamamoto Y, Komai T, Kawamura T. PSRK method for gas hydrate equilibria: I. simple and mixed hydrates. *AIChE J*. 2004;50:203–214.
22. Chen GJ, Guo TM. Thermodynamic modeling of hydrate formation based on new concepts. *Fluid Phase Equilib*. 1996;122:43–65.
23. Chen GJ, Guo TM. A new approach to gas hydrate modeling. *Chem Eng J*. 1998;71:145–151.
24. Klauda JB, Sandler SI. A fugacity model for gas hydrate phase equilibria. *Ind Eng Chem Res*. 2000;39:3377–3386.
25. Clarke MA, Pooladi-Darvish M, Bishinoi PR. A method to predict equilibrium conditions of gas hydrate formation in porous media. *Ind Eng Chem Res*. 1999;38:2485–2490.
26. Wilder JW, K Seshadri, Smith DH. Modeling hydrate formation in media with broad pore size distributions. *Langmuir*. 2001;17:6729–6735.
27. Klauda, JB, Sandler SI. Modeling gas hydrate phase equilibria in laboratory and natural porous media. *Ind Eng Chem Res*. 2001;40:4197–4208.
28. Seo Y, Lee S, Cha I, Lee JD, Lee H. Phase equilibria and thermodynamic modeling of ethane and propane hydrates in porous silica gels. *J Phys Chem B*. 2009;113:5487–5492.
29. Taylor CJ, Miller KT, Koh CA, Sloan ED. Macroscopic investigation of hydrate film growth at the hydrocarbon/water interface. *Chem Eng Sci*. 2007;62:6524–6533.
30. Uchida T, Ebinuma T, Takeya S, Nagao J, Narita H. Effects of pore sizes on dissociation temperatures and pressures of methane, carbon dioxide, and propane hydrates in porous media. *J Phys Chem B*. 2002;106:820–826.
31. Sun CY, Chen GJ, Yang LY. Interfacial tension of methane + water with surfactant near the hydrate formation conditions. *J Chem Eng Data*. 2004;49:1023–1025.
32. Nakamura T, Makino T, Sugahara T, Ohgaki K. Stability boundaries of gas hydrates helped by methane-structure-H hydrates of methylcyclohexane and cis-1,2-dimethylcyclohexane. *Chem Eng Sci*. 2003;58:269–273.
33. Englezos P, Kalogerakis N, Dholabhai PD, Bishnoi PR. Kinetics of formation of methane and ethane gas hydrates. *Chem Eng Sci*. 1987;42:2647–2658.
34. Peng BZ, Dandekar A, Sun CY, Luo H, Ma QL, Pang WX, Chen GJ. Hydrate film growth on the surface of a gas bubble suspended in water. *J Phys Chem B*. 2007;111:12485–12493.

Appendix

Sixteen pressurization paths in searching the metastable boundary pressures of four water-in-*n*-octane emulsions (denoted by $1^{\#}$, $2^{\#}$, $3^{\#}$, and $4^{\#}$ in Table 1, respectively) at four different temperatures in the presence of methane gas are given in Figures A1 to A4, respectively.

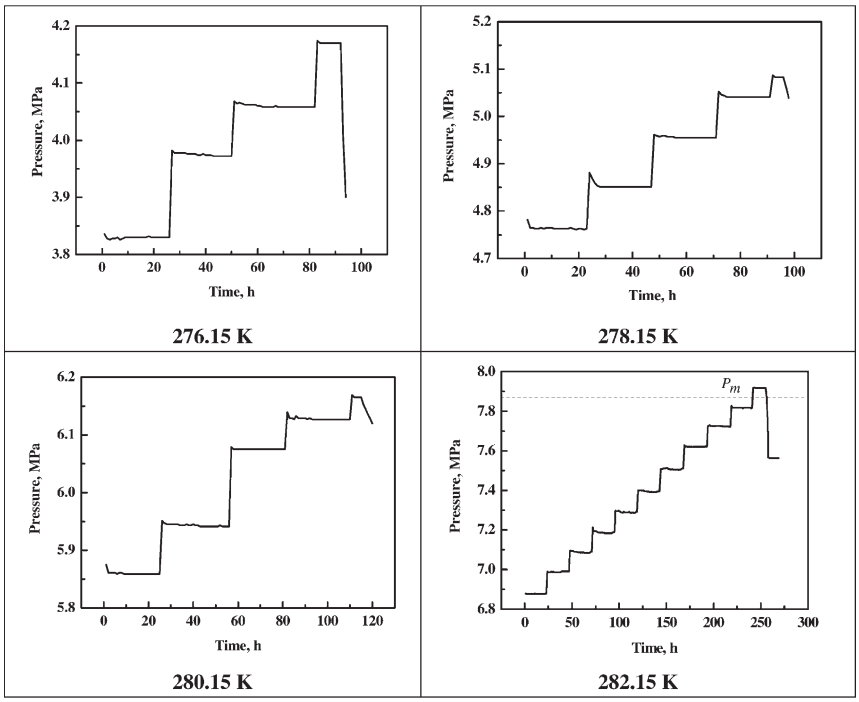

Figure A1. Pressurization paths for emulsion $1^{\#}$.

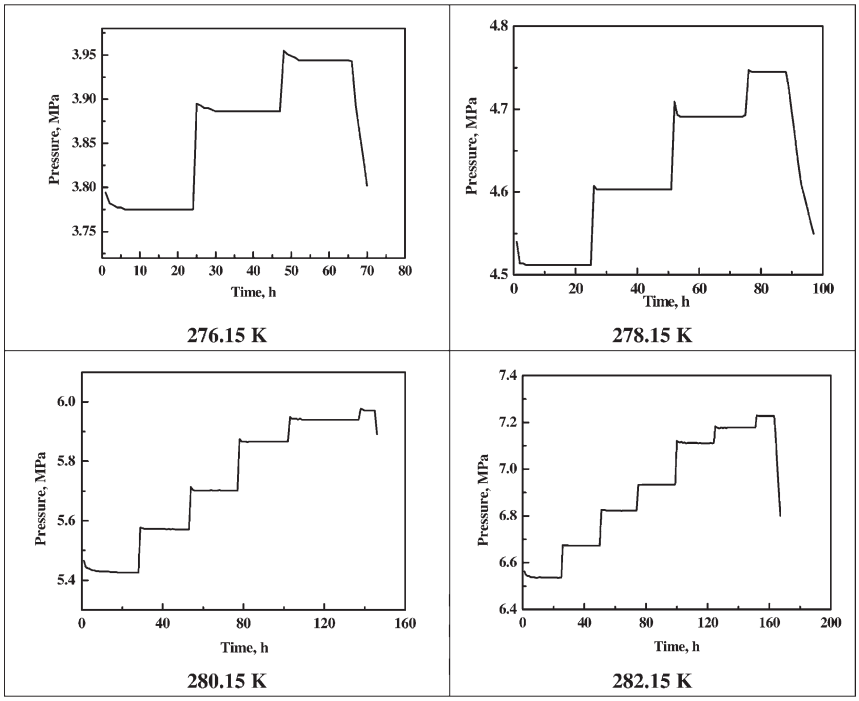

Figure A2. Pressurization paths for emulsion 2#.

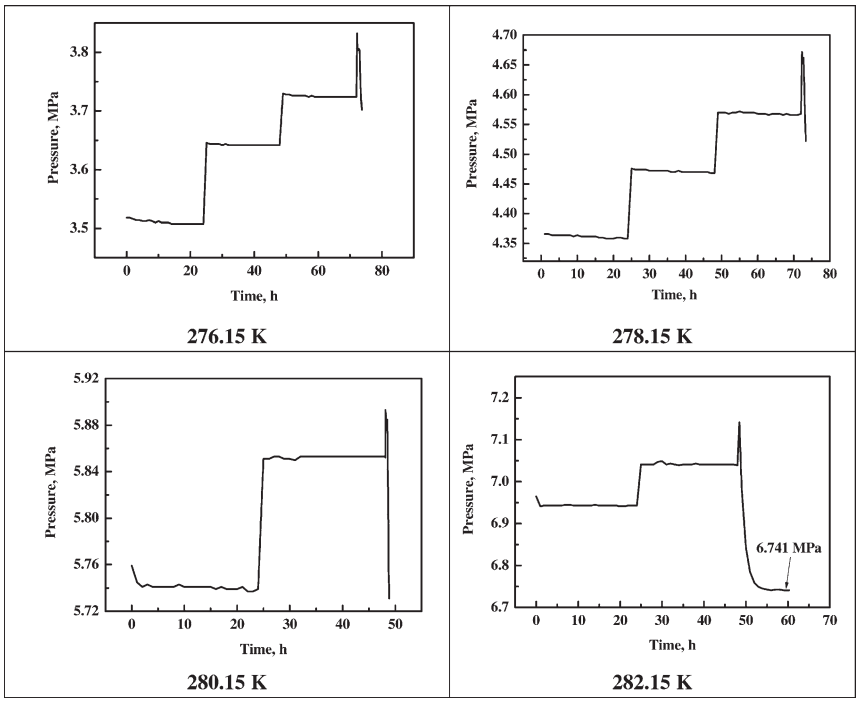

Figure A3. Pressurization paths for emulsion 3#.

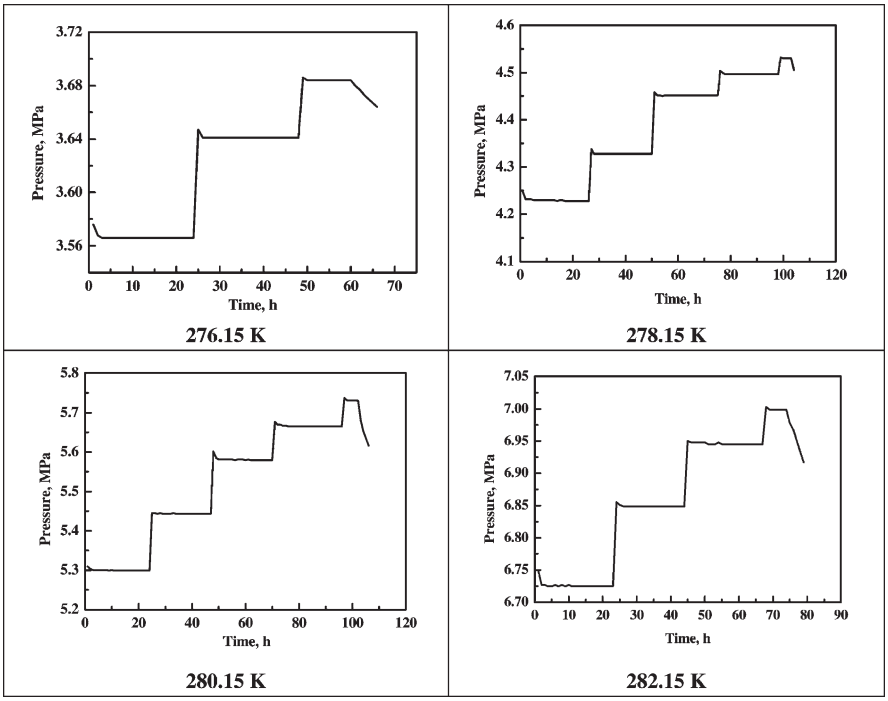

Figure A4. Pressurization paths for emulsion 4#.

Manuscript received May 16, 2011 and revision received Jun. 20, 2011.